Proceedings of the 10th
World Congress on Intelligent Control and Automation
July 6-8, 2012, Beijing, China

Design of Entry Trajectory Tracking Law for a Hypersonic Vehicle via Inversion Control

Zhiqiang Pu, Xiangmin Tan, Guoliang Fan, and Jianqiang Yi
Institute of Automation, Chinese Academy of Sciences, Beijing, 100190, China
zhiqiang.pu@ia.ac.cn

***Abstract* - A nominal altitude-velocity longitudinal entry trajectory is planned and tracked for a Generic Hypersonic Vehicle (GHV) in this paper. The entry corridor is presented which is defined by the dynamic pressure, normal acceleration, heating constraints, and the so-called Quasi-Equilibrium Glide Condition (QEGC). The flyability of the vehicle along the nominal trajectory is carefully analyzed for further validation of the selected nominal trajectory. The control scheme mainly consists of two loops: a guidance loop and an attitude loop, of which the latter is separated into the slow and fast loops with the time-scale separation theory. Inversion control is employed in these three loops, and an integration feedback approach is especially added into the inversion controller to eliminate the tracking error. Simulations demonstrate that the nominal trajectory is designed appropriately and tracked well.**

Index Terms –Hypersonic Vehicle, Entry Trajectory Tracking, Inversion Control, Integration Feedback

I. INTRODUCTION

As a lot of efforts have been made to develop next generation of Reusable Launch Vehicles (RLVs) and hypersonic military vehicles, the design of robust and practical guidance control systems for hypersonic entry vehicles has received more and more attention in these decades [1]-[2]. The entry flight, as the transition phase from cruise flight to the Terminal Area Energy Management (TAEM) phase, has to operate over a broad flight envelope. The aerodynamic characteristics and state variables within this envelope vary widely and the flight trajectory must satisfy many constraints [3]. All of these make the entry trajectory tracking to be an important but difficult problem. As a milestone, the Space Shuttle Orbiter [4] constructed a series of basic guidance and control concepts for entry vehicles, and many later researches were derived from it.

As discussed in this paper, the nominal profile tracking guidance is an efficient entry guidance method, which was exemplified by the Space Shuttle Orbiter. The centrepiece of this method relies on two main components. One is the planning of nominal profiles on the ground before mission; the other is on-board closed-loop tracking of these nominal trajectory profiles [5]. The nominal trajectories are often in the form of functions of the velocity or energy, such as drag-versus-energy trajectory and altitude-versus-velocity trajectory [5]-[6]. The reference trajectory design is an optimization problem with multiple targets and constraints, which is usually a complex work. Once reference trajectory profiles are generated, our concern should turn to design a closed-loop controller to track these planned trajectories.

Generally, entry control system includes two loops: the outer guidance loop and the inner attitude loop. The former is to design the control laws of the angle of attack and bank angle to track the planned reference trajectories. The latter is to design the control laws of the deflection angles of the elevator, aileron, and rudder such that the attitude system can track the required commands of the guidance loop. The thrust control should also be included into the attitude loop if the Reaction Control System (RCS) is used. In the literature, lots of methods aiming at entry control system design have been investigated. Ref. [6] applied model reference adaptive control to track the planned nominal altitude-velocity trajectory, but the flyability was not added into the trajectory constraints. Ref. [7] designed a control law based on a characteristic model, and [8] developed a predictive control law based on the state-dependent Riccati equations of the entry vehicle, but both only discussed the attitude loop and the reference commands were too simple to verify the controllers in practical situations. Within the last decades, dynamic inversion control, with its simplicity and practicability, has become a popular methodology in aircraft flight controller design [9]-[10], especially for aircrafts with extensive flight envelopes, like entry vehicles. It is also the approach we take in this paper.

Our objective in this paper is to address the whole design scheme of the longitudinal entry trajectory tracking for the Generic Hypersonic Vehicle (GHV) [11], including the trajectory planning, guidance control, and attitude control. As the trajectory planning gets less concern, a straight path is designed in the form of altitude-versus-velocity profile to simplify the design process. All of the entry corridor constraints are considered, and the flyability along this trajectory is analysed for further validation of the planned trajectory. As for the control problem, we first separate the attitude system into fast-state and slow-state loops with the time-scale separation theory; then inversion control is applied into the guidance, fast-state, and slow-state loops. At last, integration feedback is especially applied to eliminate the tracking errors resulting from modelling error and other uncertain factors.

978-1-4673-1398-8/12/$31.00 ©2012 IEEE

II. Problem Statement

A. Entry Model

The entry model of GHV is similar to other aircrafts. Three tips should be addressed before presenting the equations. Firstly, the rotation of the Earth is safely ignored in this paper. Secondly, as the sideslip angle is controlled to be around zero, the side force is ignored in the equations of velocity and flight-path angle. Finally, the GHV can be modelled as an axisymmetric plant as both the XOZ and XOY planes are symmetric, thus the products of inertia in these two planes are zero, which will be reflected in the roll, pitch, and yaw rate equations. The standard point-mass entry dynamics of the unpowered GHV can be described as follows [7][9]:

$$\dot{h} = V\sin\gamma \tag{1}$$

$$\dot{V} = -D/m - g\sin\gamma \tag{2}$$

$$\dot{\gamma} = \frac{1}{mV}\left[L\cos\mu - m(g - \frac{V^2}{r})\cos\gamma\right] \tag{3}$$

$$\dot{\alpha} = q - \tan\beta(p\cos\alpha + r\sin\alpha) + \frac{-L + mg\cos\gamma\cos\mu}{mV\cos\beta} \tag{4}$$

$$\dot{\beta} = p\sin\alpha - r\cos\alpha + \frac{Y\cos\beta + mg\cos\gamma\sin\mu}{mV} \tag{5}$$

$$\dot{\mu} = \frac{p\cos\alpha + r\sin\alpha}{\cos\beta} + \frac{1}{mV}(L\tan\gamma\sin\mu + L\tan\beta + Y\tan\gamma\cos\mu\cos\beta - mg\cos\gamma\cos\mu\tan\beta) \tag{6}$$

$$\dot{p} = \left[\bar{L} + (I_y - I_z)qr\right]/I_x \tag{7}$$

$$\dot{q} = \left[\bar{M} + (I_z - I_x)pr\right]/I_y \tag{8}$$

$$\dot{r} = \left[\bar{N} + (I_x - I_y)pq\right]/I_z \tag{9}$$

The nomenclature can be referred to [9]. In these equations, (1)-(3) govern the dynamics of the guidance loop, i.e. the altitude, velocity, and flight-path angle. Equations (4)-(6) govern the slow states of the attitude loop, i.e. the angle of attack, sideslip angle, and bank angle. Equations (7)-(9) govern the fast states, i.e. the roll, pitch, and yaw rate. The aerodynamic data are from the NASA technical memorandum [11]-[12]. It should be noted that, in order to cover the whole flight envelope, the aerodynamic coefficients are in the form of high-order polynomials rather than simple linear expressions, therefore the controller design may be slightly different from other researches, which will be reflected in the later section.

The air density model is as follow:

$$\rho = \rho_0 \exp(-h/h_0) \tag{10}$$

where ρ_0 is the air density of the sea level (about 1.2266 kg/m^3) and the constant $h_0 = 7315.2\ m$.

B. Tracking Problem Statement

The entry tracking problem consists of the reference trajectory planning, outer guidance control, and inner attitude control. Usually, the trajectory planning and guidance are integrated as one problem, where the former is to find a reference optimal state trajectory $x = \begin{bmatrix} h & V & \gamma \end{bmatrix}^T$ and the latter is to track this reference trajectory with $u = \begin{bmatrix} \alpha & \mu \end{bmatrix}^T$ as the control. As usual, the angle of attack is pre-designed as a function of Mach number, so the actual control of the guidance loop mainly comes from the modification of the bank angle.

The control variables α and μ of the guidance loop are virtual controls, which means it cannot directly reflect the effects of the actuators. So the objective of the attitude loop is to design control laws for the actual control variables δ_a, δ_e, and δ_r, which respectively denote the deflections of the aileron, elevator, and rudder, such that the attitude loop can track the reference commands of angle of attack and bank angle coming from the guidance loop. In addition, the sideslip angle β is usually required to keep zero.

In this paper, the GHV is at a cruise condition ($V_0 = 4590\ m/s$, $h_0 = 46540\ m$, $\gamma_0 = \beta_0 = \mu_0 = 0\ rad$, and $\alpha_0 = 0.0306\ rad$) before entry flight. The terminal point of entry is selected at $V_T = 1250\ m/s$ and $h_T = 26500\ m$. The magnitude limits of the deflections are as follow:

$$-30^\circ \le \delta_a, \delta_e, \delta_r \le 30^\circ \tag{11}$$

Other limits will be given during the design procedure.

C. Control scheme

The centrepiece of the control scheme is three inversion controllers that respectively control the guidance loop, slow-state loop, and fast-state loop. Separating the attitude loop into fast states (p, q, and r) and slow states (α, β, and μ) can simplify the controller design. This method can only be justified if there is a significant difference in time scale between the fast and slow states in the open-loop plant. It will be shown later that this is the case with GHV and most other aircrafts [9]. As the inversion controller is inherently a PD controller, two integrators with magnitude limits are added into h and α channels to eliminate the tracking errors. The configuration of the whole control system is shown in Fig. 1.

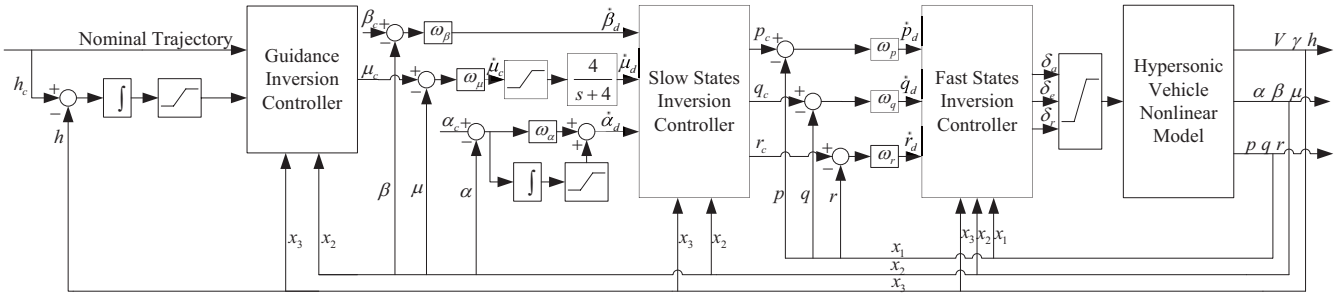

Fig. 1 The configuration of the whole control scheme

III. NOMINAL TRAJECTORY PLANNING

A. Entry Corridor

The entry flight should obey the so-called "hard limits" in terms of the maximum dynamic pressure, normal acceleration, and heating rate. To guarantee the vehicle will not rebound but directly glide to the TAEM domain, the Quasi-Equilibrium Glide Condition (QEGC) is further added to form a "soft limit". These four constraints are written as follows [5]:

$$\bar{q} \le q_{\max} \tag{12}$$

$$(L\cos\alpha + D\sin\alpha)/m \le n_{\max} \tag{13}$$

$$C_q\sqrt{\rho}V^{3.15} \le \dot{Q}_{\max} \tag{14}$$

$$L \ge m(g - V^2/r) \tag{15}$$

where $q_{\max}$, $n_{\max}$, and $\dot{Q}_{\max}$ are the maximum dynamic pressure, normal acceleration, and heating rate respectively, and C_q is a constant relying on the configuration of the vehicle. The lift and drag forces are computed as $L = 0.5\rho V^2 S_{ref} C_L$, and $D = 0.5\rho V^2 S_{ref} C_D$.

Because the nominal trajectory is in the altitude-velocity space, these four constraints should be transformed into that space accordingly. Take (12) for an example. Since $\bar{q} = 0.5\rho V^2$, where ρ is represented in (10), we can transform (12) into the altitude-velocity space as:

$$h \ge h_0 \ln\left(\frac{\rho_0 V^2}{2q_{\max}}\right) \tag{16}$$

Similarly , (13)-(15) can be transformed as follows:

$$h \ge h_0 \ln\left[\frac{\rho_0 V^2 S_{ref}(C_L\cos\alpha + C_D\sin\alpha)}{2mn_{\max}}\right] \tag{17}$$

$$h \ge h_0 \ln\left(\frac{C_q{}^2\rho_0 V^{6.3}}{\dot{Q}_{\max}{}^2}\right) \tag{18}$$

$$h \le h_0 \ln\left[\frac{\rho_0 S_{ref} C_L V^2}{2m(g - V^2/r_0)}\right] \tag{19}$$

Equations (16)-(19) constitute the entry corridor, and entry trajectories should all stay in this corridor. As the main purpose of this paper is to address the control law design rather than the trajectory planning, we choose a simple straight line from the initial point to the terminal TAEM point as the nominal trajectory, which can be expressed as:

$$h = 6V + 19000,\ 1250 \le V \le 4590 \tag{20}$$

For this vehicle, $q_{\max} = 100\ kpa$, $n_{\max} = 4g$, and $\dot{Q}_{\max} = 800\ kW/m^2$, the entry corridor and the nominal trajectory are shown in Fig. 2. It is verified that the QEGC forms the upper bound of the corridor, and the dynamic pressure, normal acceleration, and heating rate constitute the lower bound. It is also verified that the nominal trajectory (20) does stay within the entry corridor.

C. Flyability Analysis

Flyability here means that when the altitude and velocity of the vehicle are on the nominal trajectory, the required controls for the vehicle to stay on the curve should be within the capability of the vehicle [5]. From (1)-(2), we can derive that:

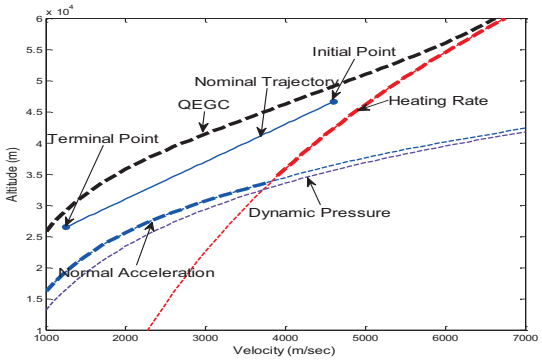

Fig. 2 Entry corridor and the nominal trajectory

$$\frac{d^2h}{dV^2} = [(m\dot{V}\sin\gamma + mV\dot{\gamma}\cos\gamma)(-D - mg\sin\gamma) - mV\sin\gamma(D\dot{h}/h_0 - \rho V\dot{V}SC_D + 2mg\dot{h}\sin\gamma/(r_0+h) - mg\dot{\gamma}\cos\gamma)]/[(-D - mg\sin\gamma)^2\dot{V}] \tag{21}$$

Equation (21) shows the effect of the bank angle appears in d^2h/dV^2 through the presence of $\dot{\gamma}$. We define the flyability corridor here as the possible values of d^2h/dV^2 when μ varies from 0 to 90 deg. The physical interpretation of the corridor boundaries is that they represent the limits of acceleration for the vehicle to pull up or dive, respectively.

For a given point on the nominal trajectory, h and V are available, thus α is obtained as a function of V. The corresponding flight-path angle γ can be derived from (1), (2), and (20) as follow:

$$\gamma = \arcsin\left[\frac{-6D}{m(V+6g)}\right] \tag{22}$$

Therefore, once a point on the reference trajectory is given, values of h, V, γ, and α are all available, thus (21) defines a relationship among d^2h/dV^2, V, and μ. When μ is set to 0 deg and 90 deg, the relationship between d^2h/dV^2 and V defines the upper and lower boundaries of the flyability corridor. As for the reference trajectory, we can easily conclude from (20) that $d^2h/dV^2 \equiv 0$.

The flyability corridor is depicted in Fig. 3. It is seen that the reference trajectory does stay within this corridor. If the velocity keeps reducing to about 1100 m/s, the trajectory will exceed the upper boundary, in which case the guidance control may fail. This situation will be validated in the later section.

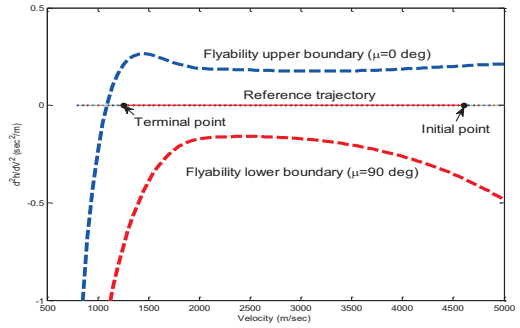

Fig. 3 Flyability corridor

IV. Guidance Control

Now that we have designed a trajectory that stays in both the entry and flyability corridors, control laws of the guidance loop should be then designed to track this trajectory.

From the guidance perspective, the angle of attack α is often preselected as a function of Mach number. At the beginning of the entry flight, α should be kept large to reduce the velocity rapidly. The dynamic pressure descends as the velocity goes down, so the reference angle of attack should descend accordingly in the end, or the vehicle cannot provide such a large angle of attack because of actuator saturation. Based on the vehicle characteristics and control capability, we design the angle of attack profile (in rad) as follow:

$$\alpha_c = \begin{cases} 0.25 & , Ma \geq 7 \\ 0.25 - 0.0065(Ma-7)^2 & , 4 < Ma < 7 \end{cases} \tag{23}$$

As α is a fixed profile, the main control comes from the bank angle. Since the nominal trajectory is in altitude-velocity space, we choose the altitude as the output, and the dynamic inversion control is applied. Differentiating (1), we obtain:

$$\ddot{h} = \dot{V}\sin\gamma + V\dot{\gamma}\cos\gamma \tag{24}$$

Substituting for $\dot{V}$ and $\dot{\gamma}$ from (2) and (3), we obtain the following affine nonlinear system:

$$\ddot{h} = f_\mu + g_\mu u \tag{25}$$

where

$$f_\mu = (-D/m - g\sin\gamma)\sin\gamma + \left[V^2/(r_0+h) - g\right]\cos^2\gamma$$

$$g_\mu = L\cos\gamma/m, \qquad u = \cos\mu$$

Now we define a new input υ and select u as follow:

$$u = (\upsilon - f_\mu)/g_\mu \tag{26}$$

Substituting (26) into (25) yields:

$$\ddot{h} = \ddot{h}_r - \ddot{e} = \upsilon \tag{27}$$

where $\ddot{e} = \ddot{h}_r - \ddot{h}$, and h_r is the reference altitude. System (27) can be controlled with diverse linear system control methods. Here we utilize the state feedback approach to assign desired closed-loop poles of the tracking error system. The control law is in the form as follow:

$$\upsilon = \ddot{h}_r - k_1 e - k_2 \dot{e} \tag{28}$$

where $e = h_r - h$, $\dot{e} = \dot{h}_r - \dot{h}$, k_1 and k_2 are the to-be-designed parameters. At last, we substitute (28) into (26) to obtain the original control law as

$$u = \left(\ddot{h}_r - f_\mu - k_1 e - k_2 \dot{e}\right)/g_\mu \tag{29}$$

The above inversion controller is inherently a PD controller, where k_1 and k_2 are the proportion and differentiation gains respectively. This controller cannot eliminate the tracking error resulting from modeling error and other uncertain factors. Therefore, we especially add an integrator with magnitude limit into (29). The final guidance control law is

$$u = \left(\ddot{h}_r - f_\mu - k_1 e - k_2 \dot{e} - k_3 \int e dt\right)/g_\mu \tag{30}$$

Because $u = \cos\mu$, the required bank angle is $\mu_c = \arccos u$.

V. Attitude Control

The guidance loop has obtained the controls α_c and μ_c to track the nominal trajectory, but these controls cannot directly reflect the action of actuators. In attitude loop, α_c and μ_c are taken as the reference commands, and the objective is to determine the final actual control laws of the actuator deflections. The attitude loop is separated into slow-state and fast-state loops with the time-scale separation theory.

A. Slow-State Loop

The slow states α, β, and μ governed by (4)-(6) have close relationship with the fast states p, q, and r. Here an implicit assumption is that the transient dynamics of the fast states occur so quickly that they have tracked their commands exactly, thus have negligible effect on the slow states.

Rewriting (4)-(6) yields

$$\begin{bmatrix} \dot{\alpha} \\ \dot{\beta} \\ \dot{\mu} \end{bmatrix} = \begin{bmatrix} f_\alpha \\ f_\beta \\ f_\mu \end{bmatrix} + g_s \begin{bmatrix} p \\ q \\ r \end{bmatrix} \tag{31}$$

where

$$f_\alpha = (-L + mg\cos\gamma\cos\mu)/(mV\cos\beta)$$

$$f_\beta = (Y\cos\beta + mg\cos\gamma\sin\mu)/(mV)$$

$$f_\mu = (L\tan\gamma\sin\mu + L\tan\beta + Y\tan\gamma\cos\mu\cos\beta - mg\cos\gamma\cos\mu\tan\beta)/(mV)$$

$$g_s = \begin{bmatrix} -\cos\alpha\tan\beta & 1 & -\sin\alpha\tan\beta \\ \sin\alpha & 0 & -\cos\alpha \\ \cos\alpha\sec\beta & 0 & \sin\alpha\sec\beta \end{bmatrix}$$

The desired values of $\dot{\beta}$ and $\dot{\mu}$ are specified by the following closed-loop dynamics:

$$\dot{\beta}_d = \omega_\beta(\beta_c - \beta) \tag{32}$$

$$\dot{\mu}_c = \omega_\mu(\mu_c - \mu) \tag{33}$$

Since μ_c is the required bank angle of the guidance loop which may change rapidly, $\dot{\mu}_c$ is put through a low-pass filter to compute $\dot{\mu}_d$ as shown in Fig. 1, which may avoid causing actuator chattering. The desired values of $\dot{\alpha}$ is similarly computed to $\dot{\beta}$. However, tracking error still remains in the channel of the angle of attack, so another integrator with magnitude limit is added, which yields

$$\dot{\alpha}_d = \omega_\alpha(\alpha_c - \alpha) + k_\alpha \int(\alpha_c - \alpha)dt \tag{34}$$

Here the bandwidths ω_α and ω_β are set at 0.4 rad/s, and ω_μ is set at 0.3 rad/s. These bandwidths are smaller than ordinary aircrafts (about 2rad/s) due to the configuration of the vehicle.

Now that $\dot{\alpha}_d$, $\dot{\beta}_d$, and $\dot{\mu}_d$ are all obtained, the fast-state commands, denoted by p_c, q_c, and r_c, are given by applying inversion to (31) as follow:

$$\begin{bmatrix} p_c \\ q_c \\ r_c \end{bmatrix} = g_s^{-1}\left(\begin{bmatrix} \dot{\alpha}_d \\ \dot{\beta}_d \\ \dot{\mu}_d \end{bmatrix} - \begin{bmatrix} f_\alpha \\ f_\beta \\ f_\mu \end{bmatrix}\right) \tag{35}$$

B. *Fast-State Loop*

The fast states p, q, and r are governed by (7)-(9). The objective of the fast-state control is to find the control laws of the actuator deflections, i.e. δ_a, δ_e, and δ_r, such that the commands p_c, q_c, and r_c can be tracked.

From the inversion control perspective, (7)-(9) should be rewritten into an affine nonlinear form. However, this cannot be derived directly because the aerodynamic coefficients in this paper are high-order polynomials instead of linear expressions [12]. Take (7) as an example. The rolling moment is $\bar{L} = \bar{q}bS_{ref}C_l$, where C_l is in the form as follow:

$$C_l = C_{l_\beta}\beta + C_{l,d_a} + C_{l,d_e} + C_{l,d_r} + C_{l_p}\left(\frac{pb}{2V}\right) + C_{l_r}\left(\frac{rb}{2V}\right) \quad (36)$$

In (36), C_{l,d_a}, C_{l,d_e}, and C_{l,d_r} are high-order polynomials of δ_a, δ_e, and δ_r, respectively. To write (7) in an affine form, we need to transform these aerodynamic coefficients into linear expressions of the deflections. Here, the first-order Taylor expansion is used to approximate the aerodynamic coefficients. This process transforms $\bar{L}$ as follow:

$$\bar{L} \approx \bar{L}_0 + L_a\delta_a + L_e\delta_e + L_r\delta_r \quad (37)$$

where $\bar{L}_0$ represents the rolling moment independent on the actuators, while L_a, L_e, and L_r represent the moments that depend on δ_a, δ_e, and δ_r respectively. Similar process yields the pitching moment $\bar{M}$ and yawing moment $\bar{N}$ as:

$$\bar{M} \approx \bar{M}_0 + M_a\delta_a + M_e\delta_e + M_r\delta_r \quad (38)$$

$$\bar{N} \approx \bar{N}_0 + N_a\delta_a + N_e\delta_e + N_r\delta_r \quad (39)$$

It should be stressed that because the Taylor expansions are updated during every sampling period, the approximations are highly reliable.

Substituting (37)-(39) into (7)-(9) gives the affine form as:

$$\begin{bmatrix}\dot{p}\\ \dot{q}\\ \dot{r}\end{bmatrix} = \begin{bmatrix}f_p\\ f_q\\ f_r\end{bmatrix} + g_f\begin{bmatrix}\delta_a\\ \delta_e\\ \delta_r\end{bmatrix} \quad (40)$$

where

$$f_p = \left[\bar{L}_0 + (I_y - I_z)qr\right]/I_x$$

$$f_q = \left[\bar{M}_0 + (I_z - I_x)pr\right]/I_y$$

$$f_r = \left[\bar{N}_0 + (I_x - I_y)pq\right]/I_z$$

$$g_f = \begin{bmatrix} L_a/I_x & L_e/I_x & L_r/I_x \\ M_a/I_y & M_e/I_y & M_r/I_y \\ N_a/I_z & N_e/I_z & N_r/I_z \end{bmatrix}$$

The desired values of $\dot{p}$, $\dot{q}$, and $\dot{r}$ are specified by the following closed-loop dynamics:

$$\dot{p}_d = \omega_p(p_c - p) \quad (41)$$

$$\dot{q}_d = \omega_q(q_c - q) \quad (42)$$

$$\dot{r}_d = \omega_r(r_c - r) \quad (43)$$

The bandwidths ω_p, ω_q, and ω_r are set at 2 rad/s, which are sufficiently beyond the bandwidths of the slow states to avoid coupling between the slow and fast dynamics. As the fast states track the commands well in simulation, there is no need to add integral terms into (41)-(43). The final control laws for the actuators are given as follow:

$$\begin{bmatrix}\delta_a\\ \delta_e\\ \delta_r\end{bmatrix} = g_f^{-1}\left(\begin{bmatrix}\dot{p}_d\\ \dot{q}_d\\ \dot{r}_d\end{bmatrix} - \begin{bmatrix}f_p\\ f_q\\ f_r\end{bmatrix}\right) \quad (44)$$

VI. Simulation Results

In simulation, 10% of parametric uncertainty is added to the model. These uncertain parameters include the air density of the sea level, the mass of vehicle, the reference wing area, the span, the mean aerodynamic chord, and the roll, pitch, and yaw moments of inertia. The performance of the inversion control with integral feedback is depicted through Fig. 4-5. Fig. 4 shows the reference and actual altitude-velocity trajectories. It is seen that the controller tracks the nominal trajectory well with a small overshoot at the beginning. Fig. 5 describes the reference and actual bank angles and angles of attack. At the beginning, because the vehicle suddenly turns from cruise to entry flight, the reference bank angle chatters sharply. However, the computed bank angle stays relatively smooth due to the low-pass filter. Without this filter, heavy chattering may happen to the actuators and the control scheme may fail. The short-term chattering of angle of attack at the beginning is also caused by the sharp changes of the reference bank angle. When the Mach number reduces to 7, the reference angle of attack goes down as the nominal profile (23) specifies.

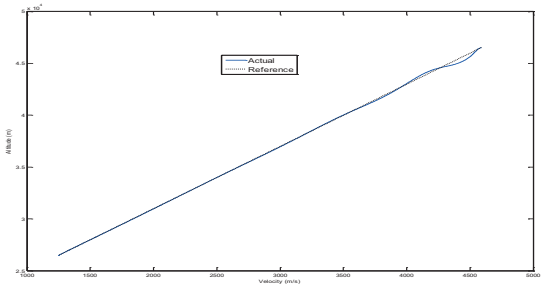

Fig. 4 Reference and actual entry trajectory

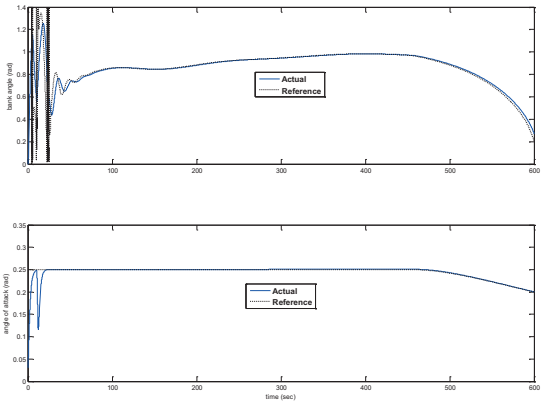

Fig. 5 Bank angle and angle of attack

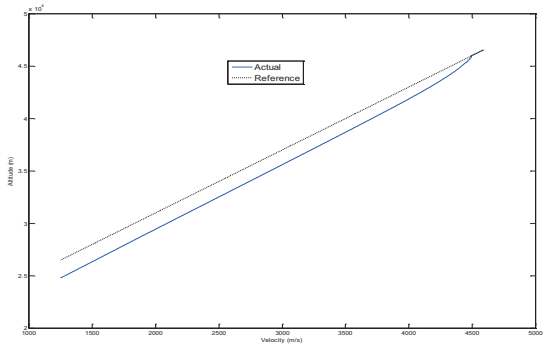

Fig. 6 Entry trajectory with the altitude integrator cancelled

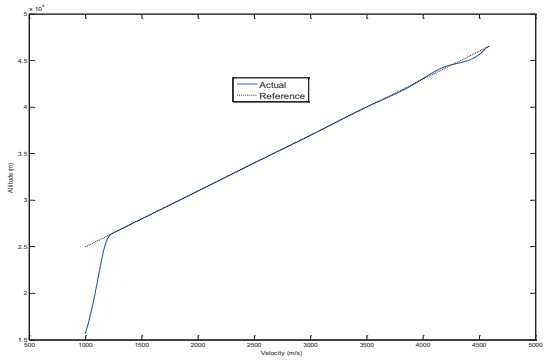

Fig. 7 Entry trajectory with the final velocity changed to 1000 m/s

To demonstrate the effects of the integral feedback, we cancel the integrator in the altitude channel. The tracking result is shown in Fig. 6. At first, there is no tracking error because the initial point is exactly on the nominal trajectory, while as time goes by, a steady error appears and cannot be eliminated. This is because the original inversion controller is inherently a PD controller which needs an integrator to completely cancel the steady error. Similar situation can also be demonstrated in the angle of attack channel.

In the end, we will validate the effect of the flyability corridor. As discussed in Section Ⅲ, the trajectory exceeds the flyability corridor when the velocity reduces to about 1100 m/s. This will not happen in our research because the terminal velocity of the entry flight is 1250 m/s. To show the influence of this corridor, we change the terminal velocity to 1000 m/s. Fig. 7 shows the reference and actual trajectories under this situation. It is seen that the controller loses its tracking ability when the velocity reduces to around 1100 m/s, then the altitude drops rapidly. This result exactly matches to our analysis in Section Ⅲ. Thus, the flyability corridor is quite an important consideration in the trajectory planning procedure.

VII. Conclusions

The entry trajectory tracking scheme for the Generic Hypersonic Vehicle involves two components: the trajectory planning and tracking control. In this paper, a nominal entry trajectory in altitude-velocity space is planned, which stays in both the entry and flyability corridors. The flyability corridor, which defines the control capability of the vehicle, is an important consideration for trajectory planning as shown in Fig. 7. As for the control system, inversion control is used in both the guidance and attitude loops. For the attitude control, the system is separated into a fast-state loop and a slow-state loop with the time-scale separation theory. In order to transform the fast-state loop into an affine system so that the inversion control can be applied, the high-order aerodynamic coefficients are approximated by the first-order Taylor expansions at each sampling point. At last, two integrators with magnitude limits are especially added into the altitude and angle of attack paths to eliminate the steady error. Simulation results indicate that the whole scheme work well for the trajectory tracking problem.

Acknowledgment

This work was supported by the grants of the National Natural Science Foundation of China (No. 60904006) and CAS Innovation Projects (No. YYYJ-1122).

References

[1] Sanjay Bharadwaj, Anil V. Rao, and Kenneth D. Mease, "Entry trajectory tracking law via feedback linearization," *Journal of Guidance, Control, and Dynamics*, vol. 21, no. 5, pp. 726-732, September-October, 1998.

[2] E. Mooij, and I. Barkana, "Stability analysis of an adaptive guidance and control system applied to a winged re-entry vehicle," *AIAA Guidance, Navigation, and Control Conference and Exhibit*, AIAA 2005-6290, 15-18 August 2005.

[3] Jennifer Georgie and John Valasek, "Evaluation of longitudinal desired dynamics for dynamic-inversion controlled generic reentry vehicles", Journal of Guidance, Control, and Dynamics, vol. 26, no. 5, pp. 811-819, September-October 2003.

[4] Jon C. Harpold, and Claude A. Graves, "Shuttle entry guidance," *Journal of Astronautical Sciences*, vol. 27, no.3, pp. 239-268, 1979.

[5] Zuojun Shen, and Ping Lu, "On-board entry trajectory planning expanded to sub-orbital flight," *AIAA Guidance, Navigation, and Control Conference and Exhibit*, AIAA 2003-5736, 11-14 August 2003.

[6] E. Mooij, "Model reference adaptive guidance for re-entry trajectory tracking," *AIAA Guidance, Navigation, and Control Conference and Exhibit*, AIAA 2004-4775, 16-19 August 2004.

[7] Zhao Zhang, Jun Hu, and Yong Wang, "Characteristic model-based reentry vehicle guidance law design," *Aerospace Control and Application,* vol. 36, no. 4, 2010.

[8] Wei Fang, and Changsheng Jiang, "Design of a predictive control law for re-entry aerospace vehicles," *Systems Engineering and Electronics*, vol. 29, no. 8, 2007.

[9] S. Antony Snell, Dale F. Enns, and William L. Garrard Jr., "Nonlinear inversion flight control for a supermaneuverable aircraft," *Journal of Guidance, Control, and Dynamics*, vol. 15, no. 4, pp. 976-984, July-August, 1992.

[10] W. R. van Soest, Q. P. Chu, and J. A. Mulder, "Combined feedback linearization and constrained model predictive control for entry flight," *Journal of Guidance, Control, and Dynamics*, vol. 29, no. 2, pp. 427-434, March-April, 2006.

[11] John D. Shaughnessy, S. Zane Pinckney, and John D. McMinn, "Hypersonic vehicle simulation model: winged-cone configuration," *NASA Technical Memorandum 102610*, NASA Langley, 1991.

[12] Shahriar Keshmiri, Richard Colgren, and Maj Mirmirani, "Development of an aerodynamic database for a generic hypersonic air vehicle," *AIAA Guidance, Navigation and Control Conference and Exhibit*, AIAA 2005-6257, 15-18 August, 2005.

[13] Hassan K. Khalil, *Nonlinear Systems*, 3rd ed., Prentice Hall, 2001, pp.505-521.